Towards Molybdenum Disulfide Exciton-Polaritons in Metallic Microcavities

Clark Embleton

An undergraduate thesis advised by Ethan Minot

Submitted to the Department of Physics, Oregon State University

In partial fulfillment of the requirements for the degree BSc in Physics

Submitted on May 19, 2020

Abstract

Exciton-polaritons are a form of light-matter coupling that have potential applications as photonic transistors and logic gates. In order for a photonic transistor or logic gate to be integrated with room temperature fiber-optic technology, excitons-polaritons need to be stable at room temperature and compatible with the red and near-infrared wavelengths used in fiber-optics communication. Transition metal dichalcogenides (TMDs) offer a promising route to realizing stable, room temperature exciton-polaritons that are compatible with fiber-optic technology. In our experiments, we have followed the steps of other researchers towards realizing TMD exciton-polaritons. Specifically, we characterized the photoluminescence of monolayer TMD molybdenum disulfide (MoS_2), built an optical microcavity that was tuned to the molybdenum disulfide emission, and transferred monolayer MoS_2 from its growth substrate to a target substrate. We found the MoS_2 exciton emission to be 1.82 eV, while the cavity mode for transverse electric polarized light could be tuned from 1.52 eV to 1.97 eV by changing the angle of light incident upon the cavity. The next steps in this experiment would be to transfer monolayer MoS_2 into a microcavity and see if polaritonic behavior can be observed. If there is evidence of exciton-polariton formation, then we could work towards realizing polaritonic devices such as optical transistors and logic gates.

Table of Contents

List of Figures

1 Introduction

Polaritons are hybrid, light-matter quasiparticles that form when light is coupled to a dipole-carrying excitation. Different dipole-carrying excitations result in different polaritons. For example, polaritons can form when light couples to plasmons (oscillations of free electrons in metals) [1], optical phonons (opposing movements of atoms in a material) [2], magnons (collective excitations of electron spin) [3], and excitons (bound states between excited electrons and holes) [4].

Exciton-polaritons have caught the attention of physicists because of their exotic behavior as Bose-Einstein condensates that can display superfluidity [5–7], applications as photonic transistors and logic gates [8,9], and lasing [10]. While a lot of pioneering exciton-polariton work has be done with traditional semiconductors, such as GaAs [5,7,11], many of these experiments were conducted at temperatures well below room-temperature [5–9,11]. These experiments were performed at low temperatures to prevent thermal energy overcoming the exciton binding energy, thereby causing the excitons to dissociate. Room-temperature exciton-polaritons have been realized in wide-bandgap semiconductors [10,12], organic semiconductors [13], and monolayer transition metal dichalcogenide (TMD) semiconductors [4].

In order to integrate exciton-polariton devices into fiber-optic based photonics, room-temperature exciton polaritons need to have wavelengths that cover the red and near-infrared spectrum used in fiber-optic technology. Wide-bandgap semiconductor exciton-polaritons cover the blue and near-ultraviolet range, which limits their telecommunication applications

[4]. Organic semiconductors can cover red and near-infrared wavelengths [14], but are generally less stable than inorganic semiconductors [15]. These drawbacks have led to scientists to look for stable room-temperature semiconductors that can host exciton-polaritons with wavelengths compatible with fiber optic technology. Transition metal dichalcogenide semiconductors are a promising candidate, because they can host exciton-polaritons with wavelengths in the telecommunication range, have excitons with a high binding energy, and are stable crystals. Lui et al. were the first to observe exciton-polaritons with a TMD semiconductor [16]. Following the work of Lui et al., TMD exciton-polaritons have been realized in distributed Bragg reflector (DBR) microcavities [17–19], metallic microcavities [20], hybrid DBR-metal microcavities [21], and waveguides [22]. For a further review of TMD exciton-polaritons see Hu and Fei [4].

In this work, I construct a metallic microcavity tuned to the exciton energy of the monolayer TMD semiconductor molybdenum disulfide (MoS_2). I optically characterize the microcavity with angle-resolved reflectance (ARR) for both transverse electric (TE) and transverse magnetic (TM) polarizations of light. I also measure the photoluminescence from monolayer MoS_2 and transfer the crystal from its growth substrate. The long-term goal of this project is to observe strong coupling between MoS_2 excitons and cavity photons.

1.1 Van der Waals Materials

Transition metal dichalcogenides are a type of van der Waals materials. Van der Waals materials have strong covalent bonds within a plane and weak van der Waals bonds between layers. Van der Waals research began with the isolation of graphene in 2004 [23]. Following the discovery of graphene many other monolayer materials were isolated [24], including TMDs.

TMDs have MX_2 stoichiometry, where M is a transition metal and X is a chalcogen (S, Se, Te). Among the TMDs, MoS_2, molybdenum diselenide ($MoSe_2$), tungsten disulfide (WS_2), and tungsten diselenide (WSe_2) show a shift from an indirect bandgap in the bulk material to a direct bandgap at the monolayer limit [25]. This facilitates more efficient photoabsorption and emission allowing for these semiconductors to be used in devices such as transistors [26], photodetectors [27], LEDs [28], and solar cells [28].

1.2 Exciton-Polaritons

There are two coupling regimes for excitons and photons: weak coupling and strong coupling. Weak coupling can be handled with perturbation theory, while strong coupling results in the formation of new eigenstates. In the case of strong coupling with excitons, two eigenstates emerge: the upper polariton branch with energy greater than the uncoupled exciton and photon and the lower polariton branch with energy less than the uncoupled exciton and photon. Exciton-polaritons are a product of this strong coupling and form when the interaction rate between the exciton and the photon is faster than the dissipation rate.

In order to reach the strong coupling regime, the cavity mode must be tuned to the exciton energy and the energy splitting between the upper and lower polariton branch, called the Rabi splitting, must be greater than the cavity mode linewidth or exciton emission linewidth [29]. The cavity mode can be adjusted by engineering the thickness of a spacer layer between the microcavity mirrors. By centering the semiconductor in the microcavity the electric field can be maximized at the semiconductor. The cavity mode linewidth narrows as the quality factor increases. The quality factor is defined to be the quotient of the resonate frequency and linewidth, which is the full width at half maximum (FWHM) [29].The quality factor is inversely

proportional to the fraction of energy lost in a single round trip, so as the quality factor increases, the energy dissipation rate decreases [29]. High quality factors are advantageous because they allow strong coupling at lower Rabi splitting. High quality factors can be obtained by using highly reflective DBR mirrors. Figure 1 diagrams the physics of an exciton-polariton.

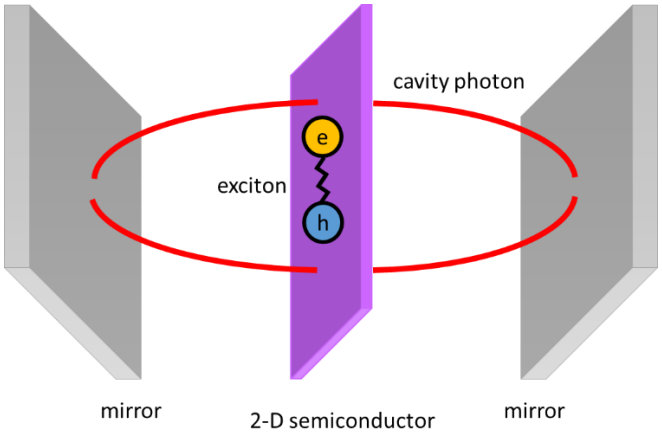

Figure 1.1: Exciton-polaritons with a 2-D semiconductor acting as a quantum well

A polariton can be described as a superposition of a cavity photon and exciton. The cavity mode can be model by [30]

$$E_{\text{cav}}(\theta) = E_{\text{cav}}(0)[1 - \frac{\sin^2(\theta)}{n_{\text{eff}}}]^{-1/2}. \quad (1)$$

$E_{\text{cav}}(0)$ is the normal incidence photon energy and n_{eff} is the effective refractive index of the spacer layer, which is different for TE and TM polarized light. For TE polarized light, n_{eff} is the refractive index of the spacer layer, n, but for TM polarized light, n_{eff} is

$$n_{\text{eff}} = \frac{n(2d_{\text{p}} + L)}{[L^2 - (2d_{\text{p}})^2]^{1/2}}, \quad (2)$$

where L is the thickness of the spacer layer and d_{p} is the plasmonic penetration depth [30]. The plasmonic penetration depth depends on the plasma frequency $d_{\mathrm{p}} = \frac{c}{\omega_{\mathrm{p}}}$, where c is the speed of light. For silver the plasma frequency is $1.36 \times 10^{16}\mathrm{Hz}$ [31].

Since the cavity mode is a function of the angle, the cavity mode can be tuned to the exciton energy making angle resolved photoluminescence (ARPL) and ARR apt for characterizing exciton-polaritons. The signature of an exciton-polariton is two dips in the ARR measurement and two peaks in the ARPL measurement. By plotting the energy of the dips (peaks) versus the angle of incident light the Rabi splitting can be determined. The Rabi splitting when the exciton energy equals the cavity mode energy is described by [29]

$$\omega_{\mathrm{Rabi}} = [4V^2 - (\gamma_c - \gamma)^2]^{1/2}. \quad (3)$$

V is a measure of the coupling strength between the cavity photon mode and exciton, while γ_c and γ parameterize the cavity photon mode and exciton losses, respectively.

2 Methods

2.1 Molybdenum Disulfide

Monolayer MoS_2 is a crystal held together by covalent S-Mo-S bonds. The structure of the crystal lattice is depicted inf Figure 2.1. Multilayer MoS_2 is held together by van der Waals forces, which makes the bulk crystal susceptible to exfoliation. While exciton-polaritons have been realized with exfoliated monolayer TMD flakes [32], chemical vapor deposition (CVD) provides more uniform monolayer coverage. CVD-grown monolayer MoS_2 flakes were provided by van der Zande's group at the University of Illinois Urbana-Champaign.

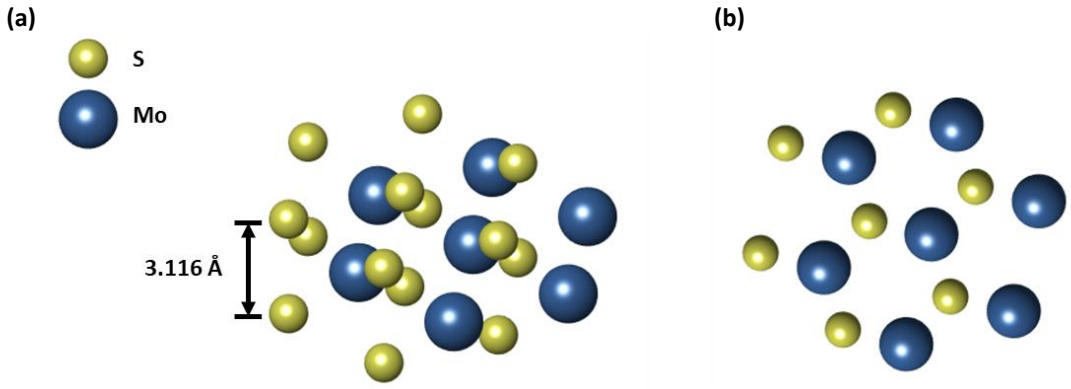

Figure 2.1 (a) A single molybdenum atom is centered in a trigonal prism of sulfur atoms. The distance between the planes defined by the two sulfur layers is 3.116 Å [33]. (b) Molybdenum and sulfur are arranged hexagonally with an offset that centers the molybdenum between three sulfur above and below.

Figure 2.2 shows the emission spectrum for monolayer MoS_2 as reported by Mak et al. [34]. There is an emission peak slightly below 1.9 eV, which corresponds to the A exciton [34]. Figure 2.3a shows the experimental setup that was used in this lab to measure the photoluminescent spectrum of MoS_2, while Figure 2.3b shows that setup used to measure and image the photoluminescence.

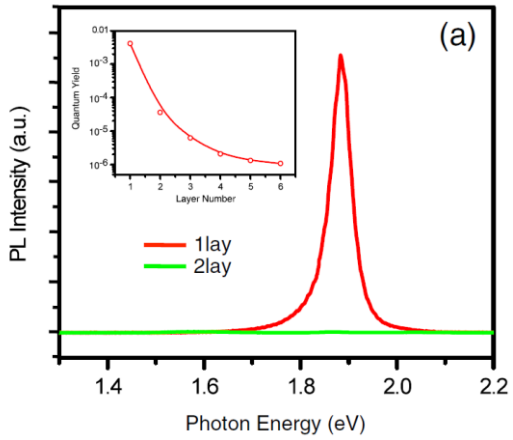

Figure 2.2 The photoluminescence spectrum from monolayer MoS_2 shows that MoS_2 has an emission peak slightly below 1.9 eV. The inset shows that the photoluminescence decreases drastically in multilayer MoS_2. This figure was adapted from Mak et al. [34].

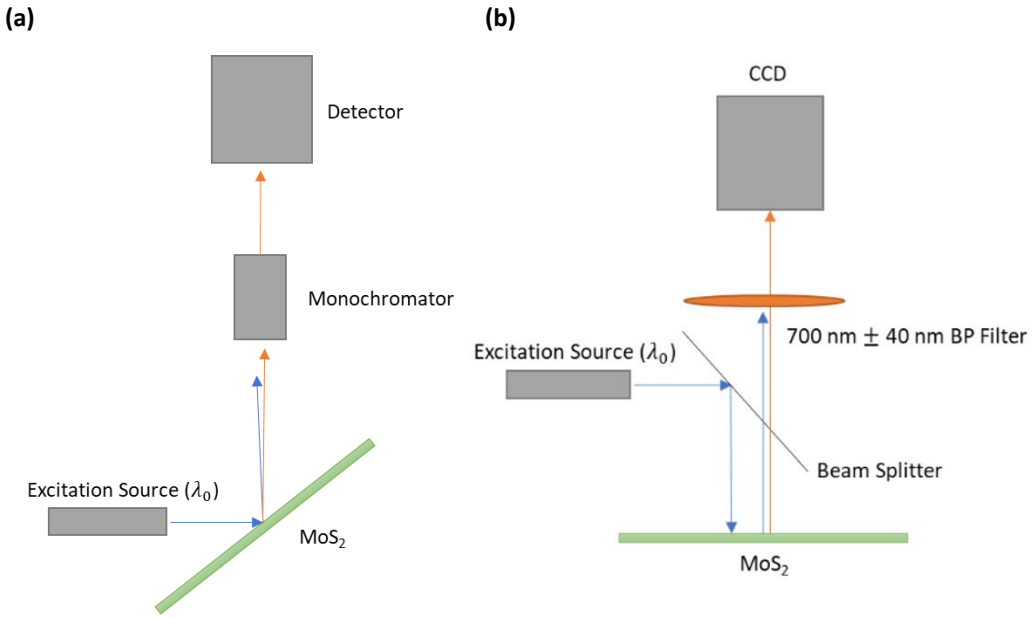

Figure 2.3 (a) The PL spectrum of monolayer MoS_2 was obtained using a 480 nm excitation source. A monochromator was used to select for the full PL spectrum while blocking the excitation source. (b) A CCD camera was used to image illuminated MoS_2 (λ_0 = 680 nm) and photoluminescent MoS_2 (λ_0 = 450 nm). A bandpass filter was used to regulate the light incident upon the CCD camera.

2.2 Microcavity Fabrication

Filmetrics' reflectance calculator [35] was used to determine the microcavity parameters necessary to host a cavity photon with an energy tuned to the MoS_2 A exciton energy as shown in Figure 2.4. The silver mirrors are designed primarily for ARR measurements as the bottom half of the cavity has 100 nm of silver on top of a glass substrate that makes ARPL measurements taken from the bottom side of the cavity difficult. A thicker layer of silver is used on the bottom half of the cavity to increase the quality factor. The cavity diagramed in Figure 2.4 has a theoretical quality factor of 80 and a cavity mode linewidth of 23.5 meV as estimated from Filmetrics' software. The Rabi splitting of MoS_2 has been reported to be about 46 meV [16], so the silver mirrors theoretically have a linewidth narrow enough to enter the strong coupling regime.

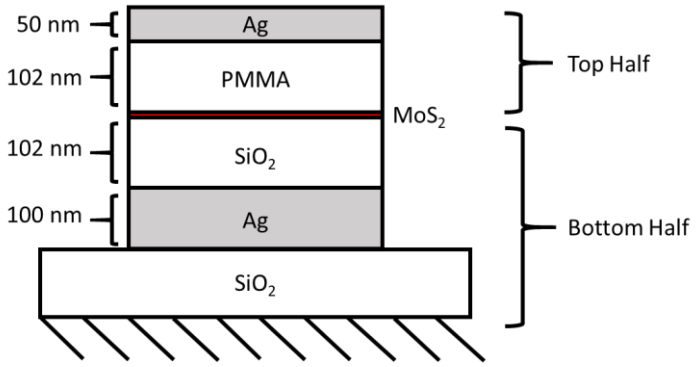

Figure 2.4 Target microcavity parameters calculated using Filmetrics' software. The refractive indices of SiO_2 are both approximately 1.5.

The spacer layer is designed to have cavity mode resonance of 1.82 eV at an angle of 50° for TM polarized light. An ellipsometer with a range of 20°-80° was used to characterize microcavities. A cavity resonant at 1.82 eV at 50° allows for the most tunability near MoS_2 photoluminescence. TE polarized light can also be tuned to the exciton emission as the higher effective index for TE polarized light stretches the spread of angle-dependent cavity mode energies according to Equation 1. Consequently, TE polarized light will have a cavity mode of 1.82 eV at angles smaller than 50°.

Microcavities were fabricated using electron beam evaporation and spin-casting. Electron beam evaporation was used to deposit the silver mirrors and silicon dioxide bottom spacer layer. Spin casting was used to put a thin film of polymethyl methacrylate (PMMA) on top of the silicon dioxide. The actual cavity had 100 nm of silver as the bottom mirror, 117 nm of SiO_2 on top of the bottom silver mirror, 120 nm of PMMA on top of the SiO_2, and a 50 nm silver top mirror.

2.3 Molybdenum Disulfide Transfer

Monolayer MoS_2 needs to be transferred to the bottom half of the microcavity before the top half is completed, which can be accomplished using the transfer method of Lu et al. [36]. Figure 2.5 shows images of successfully transferred MoS_2.

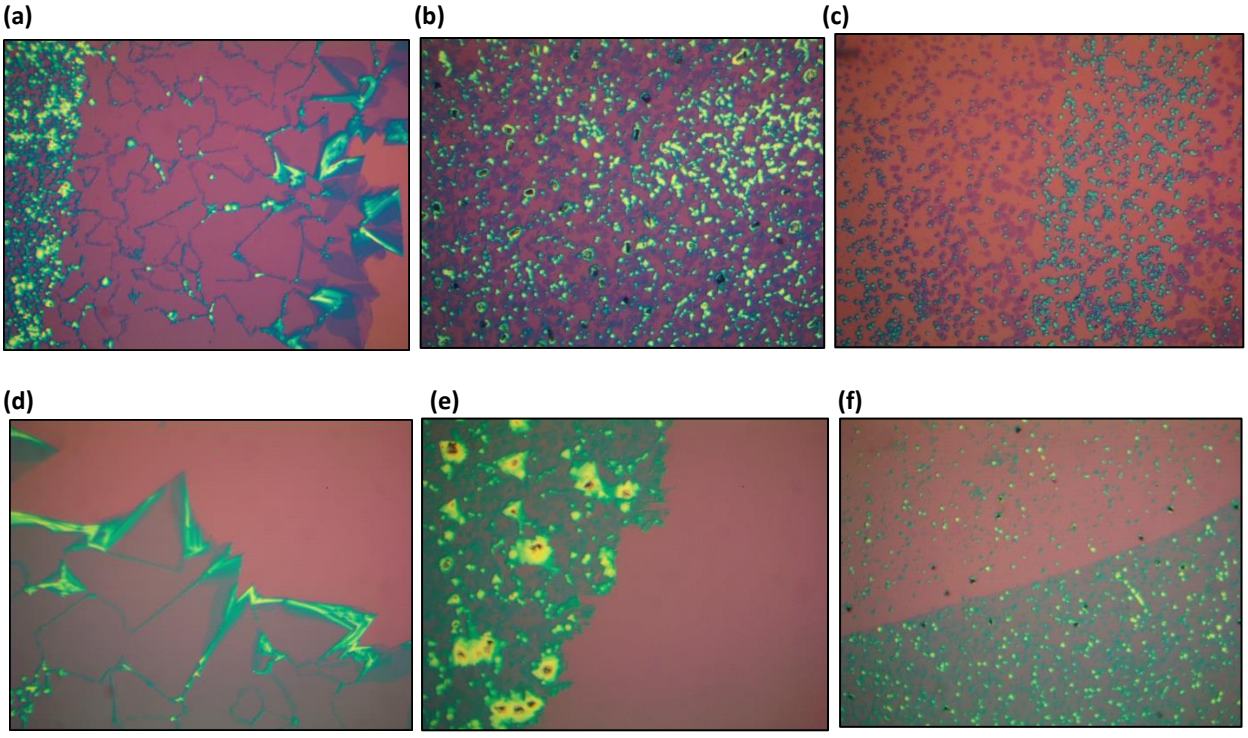

Figure 2.5 Images of MoS_2 before (a-c) and after transfer (d-f). All images were taken at 40x magnification. The edges in (e) and (f) are due to crinkling of the polymer used in the polymer-mediated transfer.

2.4 Optical Characterization

Figure 2.6a and Figure 2.6b show diagrams of the optical setups used to measure ARPL and ARR, respectively. For ARPL a 355 nm laser will be used to excite the MoS_2 and the cavity emission will be captured at various angles. For ARR a photodetector is positioned by an ellipsometer to collect the reflectance at various angles. The ellipsometer sweeps through a set of wavelengths that are incident on a sample given a wavelength range and step size. Both optical setups can measure TE and TM polarized light. In the actual experiment only ARR measurements were taken. The ellipsometer was used to collected measurements between 20°– 80° at 5° increments, while a fiber optic spectrometer was used to measure reflectance at 0°.

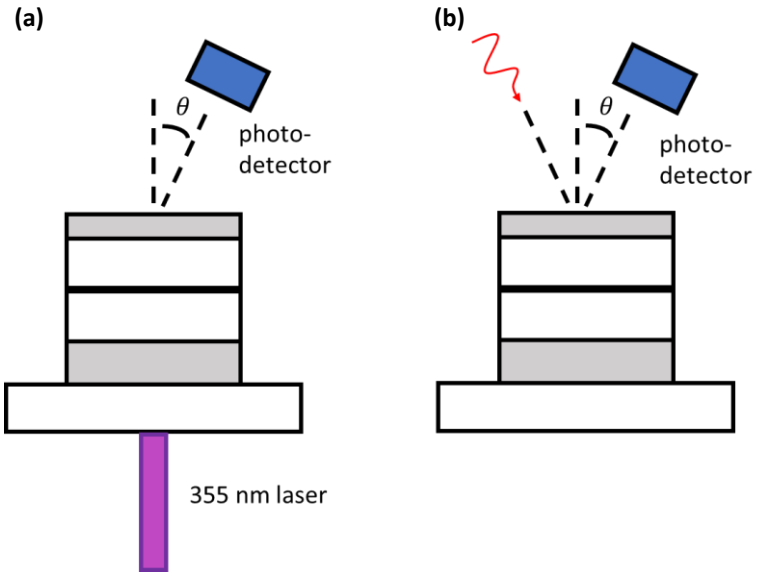

Figure 2.6 (a) A 355 nm laser excites the MoS_2 sample and the photoluminescence can be measured at various angles. (b) An ellipsometer can sweep through a set of wavelengths at each angle of incidence.

3 Results and Discussion

Figure 3.1a shows the emission spectrum from CVD grown MoS_2 taken with the setup shown in Fig. 2.3a. The MoS_2 had an emission peak near 680 nm (1.82 eV) which is close to the ~1.9 eV value reported by Mak et al. [34] and the 1.83 value reported by Splendiani et al. [37]. Reproducing previous measurements of monolayer MoS_2 exciton emission provides information that is needed to design a microcavity that can be tuned to the exciton emission. Wide field measurements were taken using the setup diagramed in Fig. 2.3b and images of illuminated and photoluminescent MoS_2 are shown in Fig. 3.1b and Fig. 3.1c, respectively. The photoluminescent MoS_2 images in Fig. 3.1c shows bright triangles with dark spots in the middle where the photoluminescence is suppressed. This can be attributed to multi-layer nucleation sites in the center of the triangular MoS_2 pieces as seen in Fig. 3.1b.

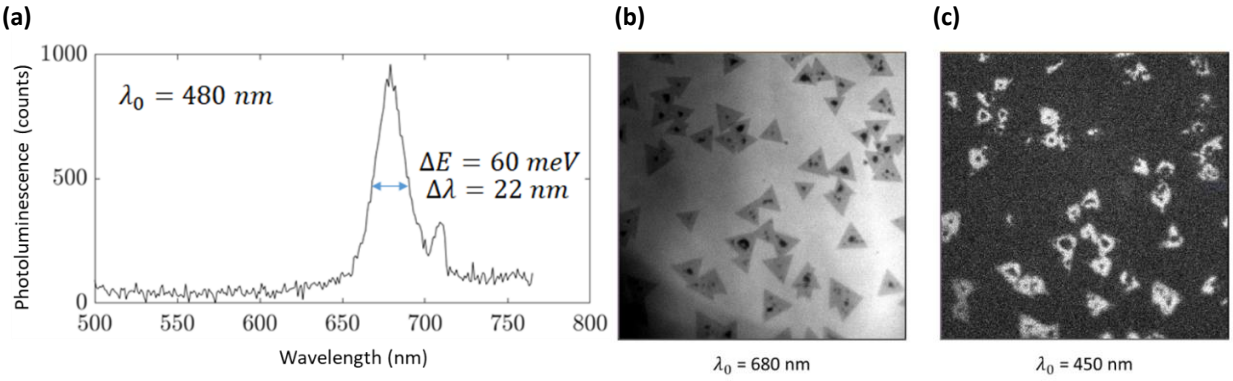

Figure 3.1 (a) The peak monolayer MoS_2 emission was around 680 nm with a linewidth of 22 nm. The excitation source, λ_0, was 480 nm. (b) The CCD camera images of illuminated MoS_2 (λ_0 = 680 nm). (c) CCD camera images of photoluminescent MoS_2 (λ_0 = 450 nm).

Angle-resolved reflectance measurements were taken on the cavity mentioned in Section 2.2 without monolayer MoS_2. The cavity mode shifts to higher energies as the angle from incidence increases. Figure 3.1c shows this cavity mode shift as a function of angle. The data in Fig 3.1c was modeled using Eq. 1 and Eq. 2. The theory curves for both TE and TM polarized light model the data well, suggesting that Eq. 1 and Eq. 2 are indeed accurate models of cavity mode angle dependence. The discrepancy between the effective indices of refraction for the theory curves and the curve used to fit the data may be due to the frequency dependence of the refractive index of the spacer layer and the slight difference between the refractive indices of SiO_2 and PMMA. As expected, without the monolayer MoS_2 inside of the cavity the signature of strong coupling, two dips in the reflectance measurements at resonance, was not observed. This is because there were no excitons for the cavity photons to couple to. No data was taken with MoS_2 inside of the microcavity because the MoS_2 sampled no longer showed signs of strong photoluminescence after a year of being in vacuum, which suggests that the samples degraded.

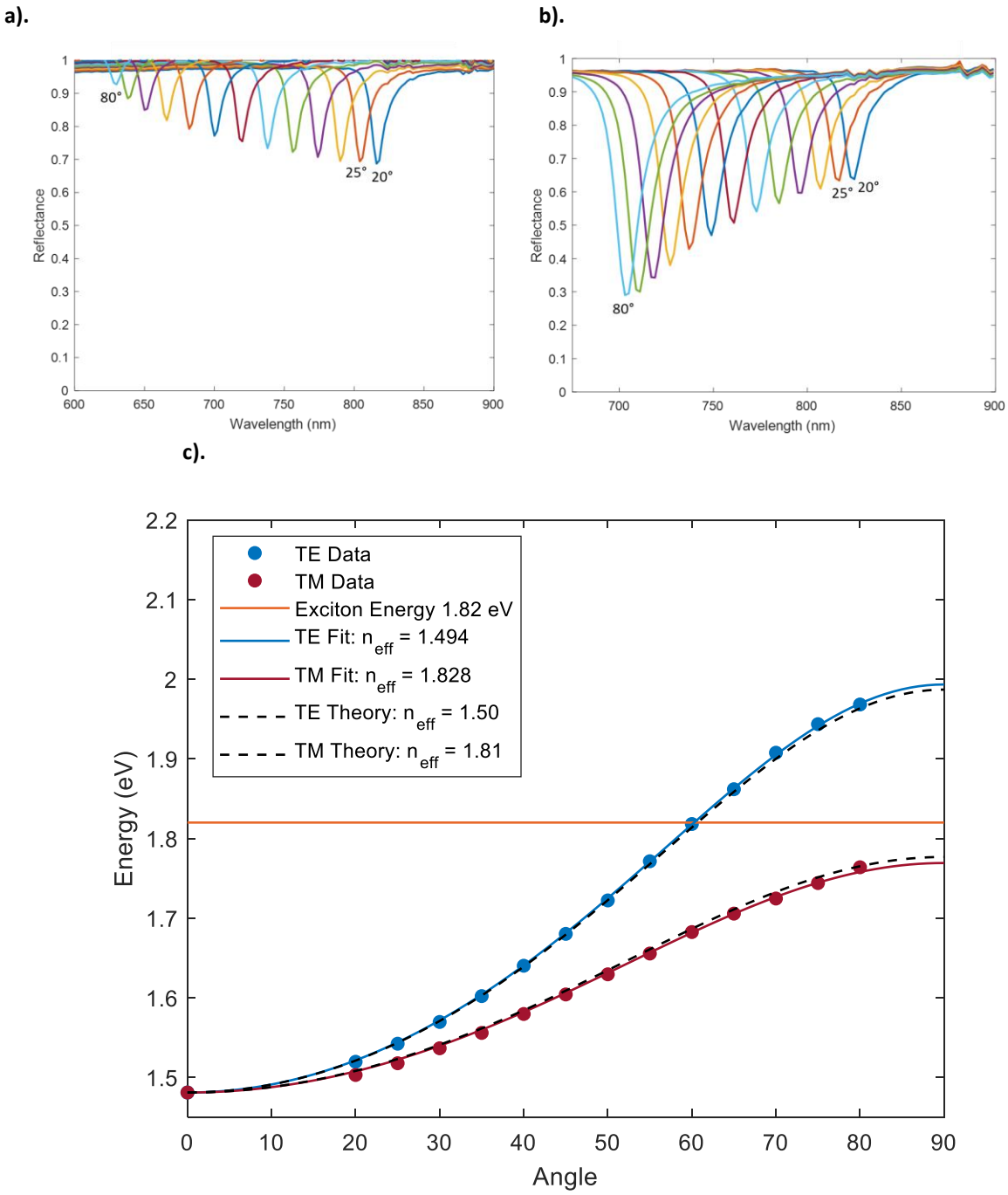

Figure 3.2 The angle-resolved reflectance spectrums for TE (a) and TM (b) polarized light were taken in 5° increments between 20° and 80°. The angle is measured from incidence, so 0° corresponds to light hitting the sample perpendicular to the plane of the sample. (c) The cavity modes correspond to the minima in the graphs in (a) and (b). Equation 1 was used to fit the data with the effective refractive index as the fitting parameter. A refractive index of 1.5 was used for the glass and PMMA spacer layer in the theory curves used to model the data. The theory curves are based on Eq. 1 and Eq. 2.

4 Conclusion

Exciton-polaritons, a strongly coupled light-matter interaction, have been used by other researchers to create devices such as optical transistors and logic gates. Such devices could be incorporated into fiber-optic technology to build photonic circuits, but these devices would need to be stable at room-temperature and cover the visible and near-infrared regions used in fiber optics. Transition metal dichalcogenides (TMDs) offer a potential path towards realizing exciton-polaritons that meet these requirements.

In this work, we took steps towards observing exciton-polaritons in molybdenum disulfide (MoS_2), a TMD that is a direct-bandgap semiconductor that can host excitons that interact strongly with light in the monolayer limit. The MoS_2 exciton photoluminescent emission was measured to have a peak around 1.82 eV. In order to couple photons to MoS_2 excitons and observe exciton-polaritons, microcavities were constructed that could be tuned to the exciton energy via the angle of incident light. Unfortunately, our single-layer MoS2 sample lost it's photoluminescent properties during the 12 months that it took to fabricate and characterize the microcavities. Therefore, we were unable to fabricate a working exciton-polariton device. Future work could transfer MoS_2 inside of a microcavity and take optical measurements to try to observe exciton-polaritons. If exciton-polaritons were observed, then the next challenge would be to research ways to construct devices such as optical transistors and logic gates with TMD exciton-polaritons.

5 Bibliography

1. S. Maier, **2007**. *Plasmonics : Fundamentals and Applications*. New York: Springer.

2. J. D. Caldwell, L. Lindsay, V. Giannini, I. Vurgaftman, T. L. Reinecke, S. A. Maier and O. J. Glembocki, **2015**. Low-loss, infrared and terahertz nanophotonics using surface phonon polaritons. *Nanophotonics*, *4*(1). pp 44-68.

3. Y. Cao, P. Yan, H. Huebl, S. T. B. Goennenwein and G. E. W. Bauer, **2015**. Exchange magnon-polaritons in microwave cavities. *Physical Review B*, *91*(9), p. 094423.

4. F. Hu and Z. Fei, **2019**. Recent Progress on Exciton Polaritons in Layered Transition-Metal Dichalcogenides. *Advanced Optical Materials*, p. 1901003.

5. H. Deng, G. Weihs, C. Santori, J. Bloch and Y. Yamamoto, **2002**. Condensation of Semiconductor Microcavity Exciton Polaritons. *Science*, *298*(5591), pp. 199–202.

6. J. Kasprzak, M. Richard, S. Kundermann, A. Baas, P. Jeambrun, J. M. J. Keeling, F. M. Marchetti, M. H. Szymańska, R. André, J. L. Staehli, V. Savona, P. B. Littlewood, B. Deveaud and L. S. Dang, **2006**. Bose–Einstein condensation of exciton polaritons. *Nature*, *443*(7110), pp. 409–414.

7. A. Amo, D. Sanvitto, F. P. Laussy, D. Ballarini, E. del Valle, M. D. Martin, A. Lemaître, J. Bloch, D. N. Krizhanovskii, M. S. Skolnick, C. Tejedor and L. Viña, **2009**. Collective fluid dynamics of a polariton condensate in a semiconductor microcavity. *Nature*, *457*(7227), pp. 291–295.

8. D. Ballarini, M. D. Giorgi, E. Cancellieri, R. Houdré, E. Giacobino, R. Cingolani, A. Bramati, G. Gigli and D. Sanvitto, **2013**. All-optical polariton transistor. *Nature Communications*, *4*, p. 1778.

9. P. G. Savvidis, J. J. Baumberg, R. M. Stevenson, M. S. Skolnick, D. M. Whittaker and J. S. Roberts, **2000**. Angle-Resonant Stimulated Polariton Amplifier. *Physical Review Letters*, *84*(7), pp. 1547–1550.

10. S. Christopoulos, G. B. H. von Högersthal, A. J. D. Grundy, P. G. Lagoudakis, A. V. Kavokin, J. J. Baumberg, G. Christmann, R. Butté, E. Feltin, J.-F. Carlin and N. Grandjean, **2007**. Room-Temperature Polariton Lasing in Semiconductor Microcavities. *Physical Review Letters*, *98*(12), p. 126405.

11. C. Weisbuch, M. Nishioka, A. Ishikawa and Y. Arakawa, **1992**. Observation of the coupled exciton-photon mode splitting in a semiconductor quantum microcavity. *Physical Review Letters*, *69*(23), pp. 3314–3317.

12. L. K. van Vugt, S. Rühle, P. Ravindran, H. C. Gerritsen, L. Kuipers and D. Vanmaekelbergh, **2006**. Exciton Polaritons Confined in a ZnO Nanowire Cavity. *Physical Review Letters*, *97*(14), p. 147401.

13. D. G. Lidzey, D. D. C. Bradley, M. S. Skolnick, T. Virgili, S. Walker and D. M. Whittaker, **1998**. Strong exciton–photon coupling in an organic semiconductor microcavity. *Nature*, *395*(6697), pp. 53–55.

14. M. Held, A. Graf, Y. Zakharko, P. Chao, L. Tropf, M. C. Gather and J. Zaumseil, **2018**. Ultrastrong Coupling of Electrically Pumped Near-Infrared Exciton-Polaritons in High Mobility Polymers. *Advanced Optical Materials*, *6*(3), p. 1700962.

15. F. So, **2010**. in *Organic Electronics: Materials, Processing, Devices and Applications*.

16. X. Liu, T. Galfsky, Z. Sun, F. Xia, E. Lin, Y.-H. Lee, S. Kéna-Cohen and V. M. Menon, **2015**. Strong light–matter coupling in two-dimensional atomic crystals. *Nature Photonics*, *9*(1), pp. 30–34.

17. S. Dufferwiel, S. Schwarz, F. Withers, A. a. P. Trichet, F. Li, M. Sich, O. D. Pozo-Zamudio, C. Clark, A. Nalitov, D. D. Solnyshkov, G. Malpuech, K. S. Novoselov, J. M. Smith, M. S. Skolnick, D. N. Krizhanovskii and A. I. Tartakovskii, **2015**. Exciton–polaritons in van der Waals heterostructures embedded in tunable microcavities. *Nature Communications*, *6*, p. 8579.

18. N. Lundt, S. Klembt, E. Cherotchenko, S. Betzold, O. Iff, A. V. Nalitov, M. Klaas, C. P. Dietrich, A. V. Kavokin, S. Höfling and C. Schneider, **2016**. Room-temperature Tamm-plasmon exciton-polaritons with a WSe 2 monolayer. *Nature Communications*, *7*(1), pp. 1–6.

19. S. Dufferwiel, T. P. Lyons, D. D. Solnyshkov, A. a. P. Trichet, F. Withers, S. Schwarz, G. Malpuech, J. M. Smith, K. S. Novoselov, M. S. Skolnick, D. N. Krizhanovskii and A. I. Tartakovskii, **2017**. Valley-addressable polaritons in atomically thin semiconductors. *Nature Photonics*, *11*(8), pp. 497–501.

20. S. Wang, S. Li, T. Chervy, A. Shalabney, S. Azzini, E. Orgiu, J. A. Hutchison, C. Genet, P. Samorì and T. W. Ebbesen, **2016**. Coherent Coupling of WS_2 Monolayers with Metallic Photonic Nanostructures at Room Temperature. *Nano Letters*, *16*(7), pp. 4368–4374.

21. L. C. Flatten, Z. He, D. M. Coles, A. a. P. Trichet, A. W. Powell, R. A. Taylor, J. H. Warner and J. M. Smith, **2016**. Room-temperature exciton-polaritons with two-dimensional WS_2. *Scientific Reports*, *6*, p. 33134.

22. B. Munkhbat, D. G. Baranov, M. Stührenberg, M. Wersäll, A. Bisht and T. Shegai, **2019**. Self-Hybridized Exciton-Polaritons in Multilayers of Transition Metal Dichalcogenides for Efficient Light Absorption. *ACS Photonics*, *6*(1), pp. 139–147.

23. K. S. Novoselov, A. K. Geim, S. V. Morozov, D. Jiang, Y. Zhang, S. V. Dubonos, I. V. Grigorieva and A. A. Firsov, **2004**. Electric Field Effect in Atomically Thin Carbon Films. *Science*, *306*(5696), pp. 666–669.

24. A. K. Geim and I. V. Grigorieva, **2013**. Van der Waals heterostructures. *Nature*, *499*(7459), pp. 419–425.

25. Q. H. Wang, K. Kalantar-Zadeh, A. Kis, J. N. Coleman and M. S. Strano, **2012**. Electronics and optoelectronics of two-dimensional transition metal dichalcogenides. *Nature Nanotechnology*, *7*(11), pp. 699–712.

26. B. Radisavljevic, A. Radenovic, J. Brivio, V. Giacometti and A. Kis, **2011**. Single-layer MoS2 transistors. *Nature Nanotechnology*, *6*, p. 147.

27. O. Lopez-Sanchez, D. Lembke, M. Kayci, A. Radenovic and A. Kis, **2013**. Ultrasensitive photodetectors based on monolayer MoS_2. *Nature Nanotechnology*, *8*(7), pp. 497–501.

28. A. Pospischil, M. M. Furchi and T. Mueller, **2014**. Solar-energy conversion and light emission in an atomic monolayer p–n diode. *Nature Nanotechnology*, *9*(4), pp. 257–261.

29. A. V. Kavokin, J. J. Baumberg, G. Malpuech and F. P. Laussy, **2017**. *Microcavities*, Second. Oxford University Press.

30. S. Kéna-Cohen, S. A. Maier and D. D. C. Bradley, **2013**. Ultrastrongly Coupled Exciton–Polaritons in Metal-Clad Organic Semiconductor Microcavities. *Advanced Optical Materials*, *1*(11), pp. 827–833.

31. M. Fox, **2010**. *Optical Properties of Solids*.

32. B. Chakraborty, J. Gu, Z. Sun, M. Khatoniar, R. Bushati, A. L. Boehmke, R. Koots and V. M. Menon, **2018**. Control of Strong Light–Matter Interaction in Monolayer WS2 through Electric Field Gating. *Nano Letters*, *18*(10), pp. 6455–6460.

33. J.-W. Jiang, Z. Qi, H. S. Park and T. Rabczuk, **2013**. Elastic bending modulus of single-layer molybdenum disulfide (MoS2): finite thickness effect. *Nanotechnology*, *24*(43), p. 435705.

34. K. F. Mak, C. Lee, J. Hone, J. Shan and T. F. Heinz, **2010**. Atomically Thin MoS 2 : A New Direct-Gap Semiconductor. *Physical Review Letters*, *105*(13).

35. **N.d.** (n.d.).

36. Z. Lu, L. Sun, G. Xu, J. Zheng, Q. Zhang, J. Wang and L. Jiao, **2016**. Universal Transfer and Stacking of Chemical Vapor Deposition Grown Two-Dimensional Atomic Layers with Water-Soluble Polymer Mediator. *ACS Nano*, *10*(5), pp. 5237–5242.

37. A. Splendiani, L. Sun, Y. Zhang, T. Li, J. Kim, C.-Y. Chim, G. Galli and F. Wang, **2010**. Emerging Photoluminescence in Monolayer MoS2. *Nano Letters*, *10*(4), pp. 1271–1275.